Journal of Neuroscience Methods 273 (2016) 160–174

Contents lists available at ScienceDirect

Journal of Neuroscience Methods

journal homepage: www.elsevier.com/locate/jneumeth

A novel approach for targeted delivery to motoneurons using cholera toxin-B modified protocells

Maria A. Gonzalez Porras[a], Paul N. Durfee[c,d], Ashley M. Gregory[a], Gary C. Sieck[a,b], C. Jeffrey Brinker[c,d,e], Carlos B. Mantilla (M.D., Ph.D.)[a,b,*]

[a] Department of Physiology & Biomedical Engineering, Mayo Clinic, Rochester, MN, United States
[b] Department of Anesthesiology, Mayo Clinic, Rochester, MN, United States
[c] Center for Micro-Engineered Materials, Advanced Materials, University of New Mexico, Albuquerque, NM, United States
[d] Department of Chemical and Biological Engineering, University of New Mexico, Albuquerque, NM, United States
[e] Advanced Materials Laboratory, Sandia National Laboratories, Albuquerque, NM, United States

HIGHLIGHTS

- Cholera toxin-B (CTB) modified protocells provide a novel delivery method to target motoneurons.
- CTB-protocells display uptake by presynaptic axon terminals at neuromuscular junctions.
- CTB-protocells showed greater motoneuron uptake compared to unmodified protocells.
- CTB-protocells constitute a promising delivery vehicle for therapy in motoneuron diseases.

ARTICLE INFO

Article history:
Received 18 July 2016
Received in revised form
12 September 2016
Accepted 13 September 2016
Available online 15 September 2016

Keywords:
Neuromuscular junction
Nanotechnology
Nanoparticles
Motoneurons
Drug delivery system
Diaphragm
Phrenic nerve
Cholera toxin B
Mesoporous silica nanoparticles

ABSTRACT

Background: Trophic interactions between muscle fibers and motoneurons at the neuromuscular junction (NMJ) play a critical role in determining motor function throughout development, ageing, injury, or disease. Treatment of neuromuscular disorders is hindered by the inability to selectively target motoneurons with pharmacological and genetic interventions.
New method: We describe a novel delivery system to motoneurons using mesoporous silica nanoparticles encapsulated within a lipid bilayer (protocells) and modified with the atoxic subunit B of the cholera toxin (CTB) that binds to gangliosides present on neuronal membranes.
Results: CTB modified protocells showed significantly greater motoneuron uptake compared to unmodified protocells after 24 h of treatment (60% vs. 15%, respectively). CTB-protocells showed specific uptake by motoneurons compared to muscle cells and demonstrated cargo release of a surrogate drug. Protocells showed a lack of cytotoxicity and unimpaired cellular proliferation. In isolated diaphragm muscle-phrenic nerve preparations, preferential axon terminal uptake of CTB-modified protocells was observed compared to uptake in surrounding muscle tissue. A larger proportion of axon terminals displayed uptake following treatment with CTB-protocells compared to unmodified protocells (40% vs. 6%, respectively).
Comparison with existing method(s): Current motoneuron targeting strategies lack the functionality to load and deliver multiple cargos. CTB-protocells capitalizes on the advantages of liposomes and mesoporous silica nanoparticles allowing a large loading capacity and cargo release. The ability of CTB-protocells to target motoneurons at the NMJ confers a great advantage over existing methods.
Conclusions: CTB-protocells constitute a viable targeted motoneuron delivery system for drugs and genes facilitating various therapies for neuromuscular diseases.

1. Introduction

Targeted delivery systems to motoneurons are critical in developing effective and safe treatments for motoneuron diseases (*e.g.* amyotrophic lateral sclerosis), as well as in understanding causes of muscle denervation (*e.g.* spinal cord injury, spinal muscular atrophy

* Corresponding author at: Joseph 4-184 W, St Mary's Hospital, Mayo Clinic, 200 First St SW, Rochester, MN 55905, United States.
E-mail address: mantilla.carlos@mayo.edu (C.B. Mantilla).

http://dx.doi.org/10.1016/j.jneumeth.2016.09.003
0165-0270/

or ageing muscle) (Boido and Vercelli, 2016; Comley et al., 2016; Dupuis and Loeffler, 2009; Hepple and Rice, 2015; Mantilla and Sieck, 2009). Despite efforts in the field, treatments remain hindered by lack of drug selectivity to neurons in the central nervous system (CNS), difficulty in targeted cellular delivery, poor penetration through biological membranes/barriers and insufficient stability (Misra et al., 2003). There is an advantage in targeting motoneurons over other CNS neurons in that they have peripherally located nerve terminals at neuromuscular junctions (NMJs). This characteristic makes motoneurons accessible to treatments that exploit retrograde neuronal transport. However, the transfer of promising molecules (*e.g.*, trophic factors) into the desired sites of action with high efficiency and uncompromised activity, while minimizing adverse reactions caused by their off-target effects, remains challenging (Weishaupt et al., 2012).

Nanoparticles are novel drug delivery systems with exceptional therapeutic potential (Simonato et al., 2013) that can encapsulate a variety of compounds and deliver them to target cells or tissues often with favorable safety profiles. In particular, mesoporous silica nanoparticles (MSNPs) have unique properties that make them a suitable treatment vehicle to target motoneurons, including: (1) the ability to independently modify pore size and the surface chemistry to enhance cargo loading when compared to other common drug delivery systems (*e.g.*, liposomes); and, (2) the possibility to engineer bio-functionality and bio-compatibility by modifying the MSNPs surface (Ashley et al., 2011; Tarn et al., 2013). MSNPs encapsulated within a supported lipid bilayer (so-called protocells) exhibit the combined beneficial features of MSNPs and liposomes with versatile cargo loading, controlled release and the possibility to introduce strategic targeting ligands in the supported lipid bilayer to enable cell specific delivery of molecular components (Ashley et al., 2011).

A number of natural toxins exist that target the nervous system and could be employed in a targeting strategy (Edupuganti et al., 2012b). Cholera toxin produced by the bacterium *Vibrio cholerae* has an atoxic subunit (CTB) formed by five identical B-subunit monomers each composed of 103 amino acids (Miller et al., 2004). CTB binds a cell-surface receptor, ganglioside GM1, present on neuronal membranes (Sheikh et al., 1999; Zhang et al., 1995), and is effectively transported retrogradely in neurons. Indeed, CTB has been extensively used as a reliable neuronal tracer (Dederen et al., 1994; Mantilla et al., 2009; Wan et al., 1982). We hypothesized that cargo loaded, CTB modified protocells (CTB-protocells) will target motoneurons and show axon terminal uptake at NMJs. In the present study, we demonstrate that CTB conjugated protocells using biotin-NeutrAvidin, predominantly target motoneurons *in vitro* compared to muscle cell controls. We also show that there is CTB-protocell uptake into nerve terminals at diaphragm muscle NMJs. In addition, we validate intracellular cargo delivery using a membrane impermeable molecule, demonstrating the efficacy of CTB-protocells as a vehicle for targeting and delivering cargo to motoneurons.

2. Materials and methods

2.1. Preparation of mesoporous silica-supported lipid bilayer nanoparticles (protocells)

2.1.1. MSNP synthesis

Fluorescently labeled MSNPs with hexagonal prismatic shape composed of close packed 2.8 nm diameter cylindrical pores were synthesized via a solution-based surfactant-directed self-assembly method, as reported by Lin et al. (2005). Briefly, MSNPs were fluorescently modified by dissolving 1 mg of rhodamine B isothiocyanate (Sigma-Aldrich, St. Louis, MO) in 1 mL of *N,N*-dimethyl formamide (DMF; Sigma-Aldrich) followed by addition of 1 μL 3-aminopropyltriethoxysilane (APTES; Sigma-Aldrich). Next, 290 mg of *n*-cetyltrimethylammonium bromide (CTAB; Sigma-Aldrich) was dissolved in 150 mL of 0.50 M ammonium hydroxide (Sigma-Aldrich) solution in a 250 mL beaker, sealed, and heated at 50 °C while stirring for 1 h. Next, 3 mL of dilute ethanolic tetraethyl orthosilicate (TEOS; Sigma-Aldrich) solution and 1 mL of RITC-APTES solution were added simultaneously to the surfactant/ammonium hydroxide solution. After 1 h of continuous stirring, the particle solution was kept at 50 °C for ~18 h under static conditions. Next, the as-synthesized MSNPs were stored in a sealed container at 70 °C for 24 h. CTAB was removed by acidic solvent extraction as described in literature (Townson et al., 2013). Briefly, MSNPs were washed and refluxed in ammonium nitrate solution, followed by wash and reflux in ethanolic HCl solution, then washed and transferred to ethanol solution for storage.

2.1.2. Supported lipid bilayer formation and CTB conjugation

The procedure used to fuse liposomes to MSNPs (protocell assembly) was based on a modified method described by Liu et al. (Ashley et al., 2011; Liu et al., 2009). Briefly, 1,2-distearoyl-*sn*-*glycero*-3-phosphocholine (DSPC; Avanti Polar Lipids, Birmingham, AL) phospholipids, cholesterol (Chol; Avanti Polar Lipids, Birmingham, AL) and 1,2-distearoyl-*sn*-*glycero*-3-phosphoethanolamine-*N*-[amino(polyethylene glycol)-2000] (DSPE-PEG2000-NH2) phospholipids were pre-dissolved in chloroform, dried under vacuum for 24 h to remove residual solvent, rehydrated in Phosphate-Buffered Saline (PBS) (Life Technologies, Grand Island, NY), bath sonicated, and passed through a 100 nm filter (minimum of 21 passes). MSNP cores (25 mg/ml) were mixed with an excess of liposomes (1:4 mass ratio of MSNP:liposomes) for 30–90 min at room temperature. To remove excess liposomes, protocells were washed twice by centrifugation (15,000×*g* for 10 min) and re-suspended in PBS. CTB was conjugated to the protocells using a NeutrAvidin/biotin conjugation strategy (Nobs et al., 2004a,c). Briefly, CTB-biotin (Life Technologies, Grand Island, NY) (50 μg in PBS) was added to NeutrAvidin modified protocells (1 mg in PBS) and incubated at room temperature for 1 h. The non-conjugated CTB-biotin was removed by centrifugation (15,000×*g* for 10 min) and protocells were re-suspended in PBS. In order to estimate the number of CTB molecules on the surface of an individual protocell, we adapted equations and values previously derived (Durfee et al., 2016). Briefly, the surface area of MSNP supported lipid bilayers was calculated as a hexagonal prism with dimensions determined from EM images and was used to determine the molar ratio of DSPE-PEG-Amine (10%) per protocell as this is the moiety that is functionalized by binding to neutravidin. Complete saturation of DSPE-PEG-Amine with neutravidin was assumed on the protocell surface, with all four neutravidin binding sites conjugated by CTB-biotin based on the absence of steric hindrance.

2.1.3. YO-PRO-1 cargo loading

To study loading and release of a small molecule drug model, YO-PRO-1 (Thermo Scientific, Waltham, MA) was chosen since it can be detected by fluorescence and is membrane impermeable. YO-PRO-1 loading was achieved by soaking MSNP cores (1 mg/ml in water) in 1% volume YO-PRO-1 (1 mM in DMSO) for 12 h at 4 °C. Protocells were assembled following the supported lipid bilayer formation and CTB conjugation method described above. YO-PRO-1 loading was quantified by bath sonicating the protocells in DMSO, followed by centrifugation (repeated twice). Supernatants were saved and pooled; the concentration was determined using a microplate reader fluorescence measurement at 480/510 nm.

2.1.4. Ultrastructural characterization of protocells

Transmission electron microscopy (TEM) was used to image the MSNP structures and surface features and cryogenic TEM (cryo-TEM) was used to visualize supported lipid bilayer formation on protocells in vitreous ice. All TEM images were acquired on a JEOL 2010 200 kV high resolution transmission electron microscope (Tokyo, Japan). The pore size and surface area were calculated following the Barret-Joyner-Halenda method and the Brunauer-Emmet-Teller equation, respectively. Zeta potential data was measured on a Malvern Zetasizer Nano-ZS (Malvern, United Kingdom) equipped with a He-Ne laser (633 nm) and Non-Invasive Backscatter optics.

2.2. Motoneuron uptake and targeting specificity of protocells in vitro

Uptake of rhodamine-labeled protocells was measured in vitro using: (1) A FlexStation 3 microplate reader system (Molecular Devices, Sunnyvale, CA) in order to evaluate the effects of varying treatment concentrations and incubation times, (2) a Nikon C1 confocal imaging system (Nikon Instruments Inc., Melville, NY) to evaluate uptake in differentiated motoneuron-like NSC-34 cells as well as in L6 muscle cells to assess targeting efficiency and specificity and (3) transmission electron microscopy (TEM) of motoneuron-like NSC-34 cells after incubation with CTB-modified protocells to assess targeted cell binding and internalization.

2.2.1. Concentration and incubation time effects on protocell uptake

Motoneuron-like NSC-34 cells were seeded onto a 96-well culture plate at a density of 2×10^4 cells per well with 100 μL of maintenance medium. Cells were cultured for 24 h at 37 °C in 5% CO_2 to allow attachment to the plate. After 24 h, the medium was exchanged for treatment medium containing protocells at 25 μg/ml or 50 μg/ml. Cells were incubated with protocells for different time intervals (3–24 h). Following treatment, cells were washed twice with PBS and resuspended in PBS. Nanoparticle fluorescence was measured using a Flexstation system. Nanoparticle free-cells were used as negative controls for each experimental condition in order to obtain background fluorescence measurements.

2.2.2. Immunohistochemistry and confocal imaging

Motoneuron-like NSC-34 cells and L6 muscle cells were plated on 4-chamber Labtek slides (Thermo Scientific) at a density of 7×10^4 cells per well (~60% confluent), differentiated for 24 h with serum deprived media (for only motoneuron-like NSC-34 cells), washed with PBS and fixed in 4% paraformaldehyde. Cells were permeabilized with 0.1% Triton™ X-100 in 0.1 M TBS and blocked with 4% donkey serum. For visualization of differentiated motoneurons, an anti-beta III tubulin antibody was used (rabbit polyclonal, ab18207; Abcam, Cambridge, MA). In L6 muscle cells, anti-laminin primary antibody was used (rabbit polyclonal, L9393; Sigma Aldrich). Both were followed by secondary antibody Cy5-conjugated anti-rabbit (Jackson Immunoresearch, West Grove, PA). Motoneuron-like NSC-34 cells and L6 muscle cells were counterstained with DAPI dye and cover slipped with Fluorogel (Electron Microscopy Sciences, Hatfield, PA). Cells were imaged using a Nikon C1 confocal microscope (Nikon Instruments Inc.) equipped with argon (488 nm) and solid state (561 and 640 nm) lasers and appropriate filter combinations. Rhodamine-labeled protocells were imaged with a 40× and 60× oil immersion lens (NA 1.3 and 1.4, respectively). Laser intensity, confocal aperture, and photomultiplier gain were kept constant across samples. NIS-Elements software (Nikon Instruments Inc.) was used for image processing and analysis. Differentiated motoneurons were selected based on the expression of beta III tubulin. The fluorescence intensity of rhodamine-labeled protocells and YO-PRO-1 cargo were quantified for cells treated with either CTB-modified or unmodified protocells. Based on control cells, the background fluorescence was subtracted. The area of protocells colocalized with beta III tubulin and DAPI was measured in each plane of the z-stack comprising the cell. YO-PRO-1 total fluorescence intensity per cell was normalized by cell area.

2.2.3. TEM of motoneurons after CTB-protocell treatment

NSC-34 motoneuron-like cells were cultured 24 h prior to the experiment on 4-chamber Labtek slides, (Thermo Scientific) at a density of 7×10^4 cells per well (~60% confluent). After motoneuron differentiation, cells were incubated with CTB-protocells for 24 h and fixed in Trump's fixative (1% glutaraldehyde and 4% formaldehyde in 0.1 M phosphate buffer, pH 7.2). Cells were then rinsed for 30 min, three times, in 0.1 M phosphate buffer, pH 7.2, followed by a 30 min postfix in phosphate-buffered 1% osmium tetroxide (OsO_4). After rinsing three times in distilled water for 30 min, cells were stained with 2% uranyl acetate for 15 min at 60 °C. The cells were then rinsed in distilled water, dehydrated in progressively higher concentrations of ethanol and 100% propylene oxide, and embedded in Spurr's resin. Thin (100 nm) sections were obtained using Leica EM UC7 ultramicrotome (Buffalo Grove, IL), then placed on 200 mesh copper grids, and stained with lead citrate. Micrographs were acquired on a JEOL JEM-1400 TEM (Tokyo, Japan) operating at 80 KV.

2.3. Evaluation of cytotoxicity and cell proliferation following protocell treatment

The CytoTox-Glo (Promega, Madison, Wisconsin) cytotoxicity assay was used to assess CTB-protocell toxicity. The assay measures dead-cell protease activity using a luminogenic peptide substrate. Briefly, NSC-34 cells were incubated with two different concentrations (25 μg/ml or 50 μg/ml) of YO-PRO-1 loaded CTB-protocells for 3, 6 and 24 h. Following the manufacturer's protocol, luminescence of dead-cell protease activity (related to membrane integrity) was read after CTB-protocell treatment prior to and following addition of a lysis reagent. The ratio of luminescence of dead cell to total cell luminescence was calculated for each condition to determine the percentage of dead cells after treatment. In order to evaluate cell viability, the CyQUANT NF cell proliferation assay kit (Molecular Probes, Inc, Eugene, OR) was used in NSC-34 cells treated with 50 μg/ml of CTB-protocells for 24 h. This assay determines cell number by measuring cellular DNA content via fluorescent dye binding (485 nm Ex/530 nm Em). For both assays, a 96-well imaging plate reader with robotic pipetting capabilities (FlexStation) was used. Untreated cells with serum deprived media were used as control.

2.4. Assessment of protocell uptake in diaphragm muscle-phrenic nerve preparations

The diaphragm muscle with the phrenic nerve attached was bilaterally dissected from adult male rats and stretched to optimal length (~1.5 × resting length) on a silicone rubber–coated dish (Sylgard; DowCorning, Midland, MI). Diaphragm muscle-phrenic nerve preparations were incubated at 37 °C (5% O_2, 95% CO_2) for 24 h in DMEM (Sigma-Aldrich, D6421) containing either CTB-targeted, non-targeted protocells (50 μg/ml) or no treatment control. All preparations were then incubated at room temperature for 45 min in 0.1 M PBS containing 1 mM Alexa Fluor 488 conjugated α-bungarotoxin (Invitrogen, Carlsbad, CA). Following sequential rinses in 0.1 M phosphate-buffered saline, preparations were fixed using 4% paraformaldehyde for 2–3 h. Preparations were then immunostained using anti-synaptophysin (1:200, overnight)

Table 1
Hydrodynamic diameter and Z-potential of unloaded and YO-PRO-1 loaded MSNPs cores, protocells and CTB-modified protocells.

	Hydrodynamic Diameter (nm) (Polydispersity Index)		*Zeta potential (mV)*	
	Unloaded	YO-PRO-1 Loaded	Unloaded	YO-PRO-1 Loaded
MSNP core	109.1 ± 0.4 (0.055 ± 0.024)	1596.0 ± 131.5 (0.446 ± 0.019)	−17.5 ± 1.97	−17.8 ± 1.44
Non-targetedProtocells	140.1 ± 1.5 (0.154 ± 0.010)	124.4 ± 0.9 (0.118 ± 0.002)	−5.11	−5.24
CTB-Protocells	154.7 ± 2.1 (0.246 ± 0.004)	133.7 ± 1.5 (0.172 ± 0.016)	–	−5.22

Measurements for MSNP cores were conducted in H_20 and those for protocells in PBS.

and the appropriate Alexa Fluor 647-conjugated secondary antibody (1:300), all in 0.5% Triton X-100 (Sigma-Aldrich) in 1 M Tris-buffered saline at room temperature. Preparations were stored in TBS until imaging.

2.4.1. Neuromuscular junction confocal imaging and analysis

Diaphragm NMJs were visualized using a Nikon C1 confocal microscope (Nikon Instruments Inc.). Images were obtained using a 40 × 0.8 NA water immersion lens at 0.3 μm step size. Simultaneous three-channel detection was possible using appropriate dichroic and filter combinations to separate Alexa Fluor 488-bungarotoxin labeled motor end-plates, Cy5-labeled presynaptic terminals and rhodamine-conjugated protocells. Imaging and acquisition parameters (*e.g.*, laser intensity, confocal aperture, photomultiplier gain, and dark current) were fixed so that relative changes in fluorescence intensity could be reliably measured across experimental conditions. In order to avoid problems with fluorescence dispersion across a thick water interface in this live preparation, NMJs located superficially within the diaphragm were randomly selected for imaging (~35 per preparation).

A region of interest (ROI) outlining the motor end-plate of each NMJ was drawn from the maximum intensity projection in Nikon Elements (Universal Imaging, Downingtown, PA). Within this ROI, the protocell fluorescence intensity was examined in each plane of the z-stack comprising the NMJ. The mean fluorescence intensity for each motor end-plate (within its defined ROI) was measured and the background subtracted. The volume of apposition of CTB-protocells with pre-synaptic structures was determined from the intersection of the two binarized volumes using a customized algorithm in MetaMorph, as previously reported (Alvarez-Argote et al., 2016; Greising et al., 2015; Mantilla et al., 2014; Sieck et al., 2012)

2.5. Statistical analyses

All statistical evaluations were performed using standard statistical software (JMP 10.0, SAS Institute Inc., Cary, NC). Differences between treatment groups were examined using one-way analysis of variance, followed by Tukey-Kramer HSD test when appropriate. Statistical significance was established at the $p < 0.05$ level. All experimental data are presented as mean ± SE, unless otherwise specified.

3. Results

3.1. Physicochemical characterization of protocells modified with CTB

Synthesized MSNP cores and protocells were characterized by dynamic light scattering, TEM, cryo-TEM and zeta potential. Hexagonal MSNPs cores were obtained of uniform size (~110 nm) evident by a low polydispersity index (Table 1) and TEM imaging (Fig. 1A). Fusion of a lipid bilayer to silica cores was achieved by adding the highly lipophilic MSNP framework to liposomes in aqueous buffer (PBS), permitting spontaneous fusion largely driven by electrostatic interactions and van der Waals attractive forces (Ashley et al., 2011; Savarala et al., 2010, 2011). Formation of a supported lipid bilayer around the MSNP core resulted in an ~15% increase in hydrodynamic diameter (Table 1) and evidence of a thin, conformal bilayer (~5 nm thick), visible in the cryo-TEM images of protocells (Fig. 1B). Loading of YO-PRO-1 resulted in MSNP aggregation (Table 1), likely the result of an electrostatic attractive force

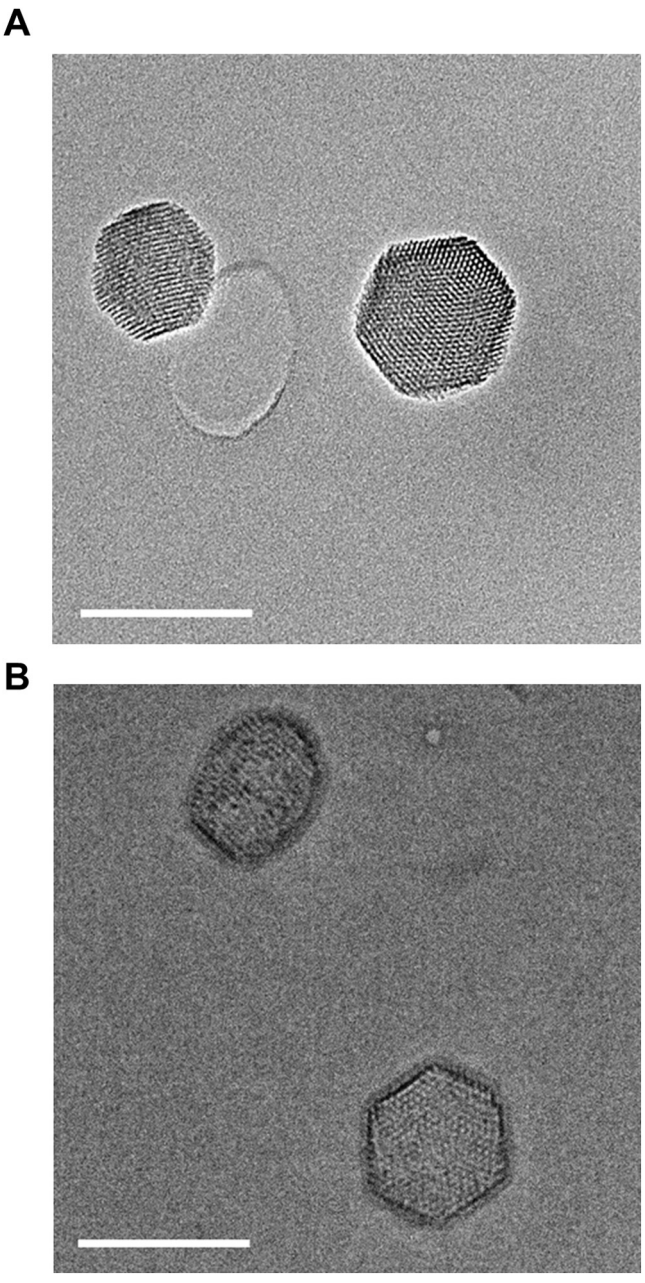

Fig. 1. (A) Representative transmission electron microscopy (TEM) image of hexagonal anisotropic MSNPs and (B) CryoTEM image of protocells. Scale bar 100 nm.

between the silanol groups in the MSNPs and the net positive charge of YO-PRO-1. With the addition of liposomes and by increasing the ionic strength of the fusion conditions, aggregation was prevented such that MSNP supported lipid bilayers simultaneously stabilize the MSNPs and encapsulate the YO-PRO-1 cargo inside. Resulting YO-PRO-1 loaded protocells were uniform in size based on hydrodynamic diameter and polydispersity index (Table 1). With 1% volume YO-PRO-1 (1 mM in DMSO) to MSNPs (1 mg/ml in H_2O), a 25% loading efficiency was obtained, calculated after disrupting protocell membranes and measuring the YO-PRO-1 concentration in the supernatant. The high encapsulation efficiency is attributed to the small size of YO-PRO-1 and attractive electrostatic interactions with the MSNP mesoporous surfaces. The incorporation of a biotinylated CTB-targeting moiety to the protocell surface resulted in a hydrodynamic diameter increase of ~10 nm (Table 1). Assuming 100% conjugation efficiency, the maximum number of CTB molecules conjugated to the surface of a single protocell is $7.36 * 10^3$.

To investigate the stability of MSNPs and protocells, z-potential measurements were performed. The values obtained were ~−18 mV and ~−5.2 mV for MSNPs cores and protocells, respectively (Table 1). While a low zeta potential value is associated with electrostatic instability, zwitterionic protocells exhibit sustained size stability in PBS due to their zwitterionic surface and water hydration (Butler et al., 2016). The change in z-potential value following fusion of the supported lipid bilayer indicated successful protocell assembly. Coating with CTB did not change z-potential values, suggesting preserved stability of CTB-protocells.

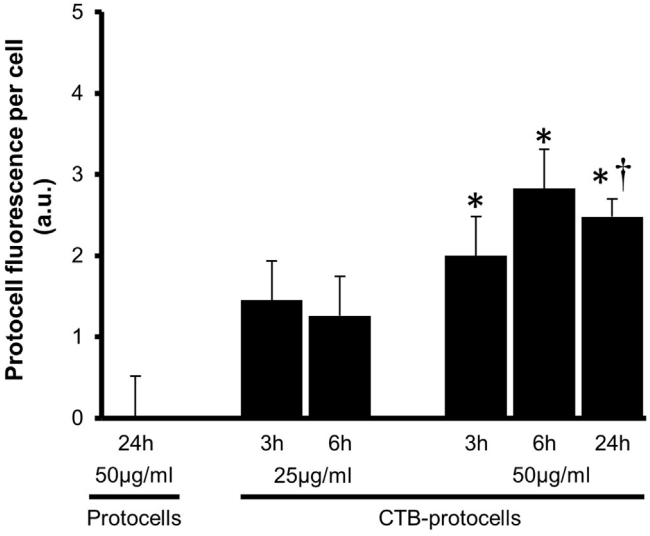

Fig. 2. Effect of incubation time, concentration and CTB modification on protocell uptake. Protocell fluorescence per cell was measured after different incubation times and protocell treatment concentrations. Significant CTB-protocell fluorescence was observed with 50 µg/ml after 3 h of incubation. No further increase was observed with longer periods of incubation. (*, $p < 0.001$ compared to control cells). After a 24 h incubation with CTB modified and unmodified protocells (50 µg/ml), increased uptake of CTB-protocells was evident compared to unmodified protocells, which showed minimal evidence of uptake (†, $p = 0.008$). Mean ± SE values were obtained from two separate experiments carried out in triplicate.

3.2. Conjugation of protocells with CTB increases uptake by cultured motoneurons

Protocell uptake was assessed as a function of incubation time and nanoparticle concentration in NSC-34 cultured cells at stable cell density (2×10^4 cells/well) using a robotic microplate reader (~5 replicates per each of 3 plates). Previous studies demonstrated CTB binding to GM1 present in NSC-34 cells (Matsumoto et al., 1995). Protocell uptake, measured as the total fluorescence per cell, was dependent on concentration and incubation time ($F_{5,83} = 15.4$; $p < 0.001$). Significantly greater CTB-protocell uptake was observed with 50 µg/ml compared to 25 µg/ml. Significant uptake was observed after 3 h of incubation and no further increase was observed with longer periods of incubation (6 and 24 h) (Fig. 2). After a 24 h incubation with 50 µg/ml of protocells or CTB-protocells, significantly greater uptake was evident with CTB modification compared to unmodified protocells ($F_{1,35} = 41.4$; $p < 0.001$) (Fig. 2).

Protocell fluorescence labeling allowed quantitative assessment of cell uptake as monitored by confocal imaging. Cultured NSC-34 motoneurons were visualized using confocal microscopy and identified as differentiated based on neurite outgrowth, consistent with previous studies (Eggett et al., 2000; Maier et al., 2013a). NSC-34 cells that were not differentiated were primarily small and rounded. Neuronal differentiation was further confirmed by immunofluorescence staining for beta III tubulin which is essential throughout neuronal differentiation (Fanarraga et al., 1999). The relative amount of intracellular protocells in differentiated motoneurons was quantified by the volume occupied by protocells in each cell after background subtraction. After protocell treatment for 24 h, differentiated motoneurons in culture showed significant CTB-protocell uptake at cell soma and dendrites compared to unmodified protocells (Fig. 3). Intracellular volume occupied by CTB-protocells was ~2.5-fold greater than that occupied by unmodified protocells ($F_{1,20} = 6.7$; $p = 0.018$) (Fig. 3C). TEM images show internalization of CTB-protocells by NSC-34 motoneuron-like cells after 24 h treatment of CTB-protocells (Fig. 4). CTB-protocell internalization was clearly visible in the cell periphery (Fig. 4A), as well as in the cytoplasm (Fig. 4B). Interestingly, CTB-protocells were not detected within larger vacuoles compartments, identified in TEM images as lysosomes (Luzio et al., 2007; Qiu et al., 2015), suggesting that these protocells can be found outside the *endo*-lysosomal compartments after 24 h of incubation (Fig. 4C).

3.3. CTB modification of protocells confers motoneuron cell specificity

To evaluate the targeting potential of CTB-protocells, motoneuron-like NSC-34 and L6 muscle cells were used. Treatment with 15 µg/ml of Alexa 488 CTB for 24 h was used in order to validate the CTB internalization by these two cell lines (Fig. 5A and B). The number of cells with CTB fluorescence was quantified based on a fluorescence threshold, which was set based on images of control untreated cells. L6 muscle cells did not exhibit evidence of CTB uptake (less than 1% of ~1000 cells counted), while most NSC-34 cells displayed evidence of CTB uptake (65%) (Fig. 5C). Ganglioside expression reportedly increases with motoneuron differentiation (Silani et al., 1993). Thus, CTB uptake by cultured cells was evaluated based on evidence of differentiation. Overall, the proportion of NSC-34 cells exhibiting CTB uptake was 20% greater for differentiated than undifferentiated cells ($n = 2$ experiments, 5 images per experiment and ~30 cells per image for a total of ~300 cells per group). CTB uptake in NSC-34 cells was also evaluated with different concentrations of Alexa 488 CTB (1.5, 15, and 150 µg/ml). Increasing CTB concentration did not result in increased uptake ($p < 0.001$) (Fig. 5D).

Specificity of protocell uptake was evaluated in cultured NSC-34 and L6 cells treated for 24 h with 50 µg/ml of unmodified or CTB-protocells (Fig. 5). Uptake was measured as the number of cells displaying internalized protocell fluorescence divided by the total number of cells in each randomly selected image. The proportion of cultured motoneurons displaying protocell uptake was 14 ± 4% for unmodified and 56 ± 4% for CTB-protocells, respectively ($n = 3$ experiments, 8 images per experiment and ~40 cells per image for

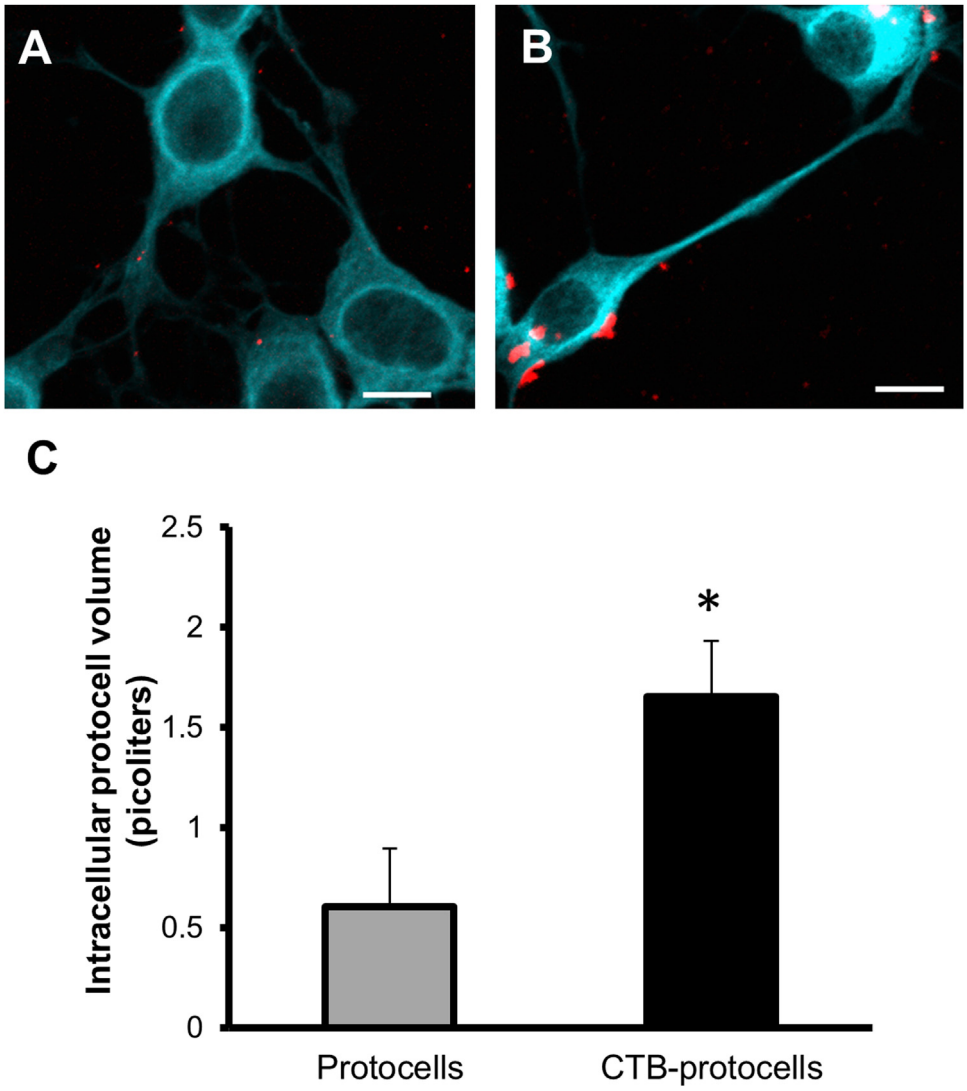

Fig. 3. Confocal microscopy images of cultured NSC-34 motoneuron-like cells demonstrating intracellular uptake of protocells. Uptake of (A) unmodified protocells and (B) CTB-protocells in differentiated NSC-34 cells stained with beta III tubulin (light blue); bar 10 μm. (C) Quantitative analysis of intracellular volume occupied by protocells (50 μg/ml; 24 h incubation) in cultured NSC-34 cells was significantly greater in CTB-protocells (*, $p = 0.008$). Mean ± SE values were obtained from 2 different experiments, 5 images per experiment and ~30 cells per image for a total of ~300 NSC-34 cells analyzed per group. (For interpretation of the references to colour in this figure legend, the reader is referred to the web version of this article.)

a total of ~1000 cells per group) (Fig. 5A and C). The proportion of cultured muscle cells displaying protocell uptake was 10 ± 1% for unmodified and 8 ± 1% for CTB-protocells, respectively (n = 3 different experiments, 4 images per experiment and ~480 cells per image for a total of ~6000 cells counted) (Fig. 5B and C).

3.4. CTB-protocells display cargo release in motoneurons

Delivery of small molecules by CTB-protocells was assessed using encapsulated YO-PRO-1, a monomeric cyanine nucleic acid stain that is unable to enter cells in the absence of apoptosis. No treatment was used as the negative control to establish background and auto fluorescence. Cells treated with CTB-protocells had significant greater YO-PRO-1 fluorescence per cell (Fig. 7A) than unmodified protocells (Fig. 7B); and both treatments showed significantly greater intracellular fluorescence compared to negative control ($F_{2,27} = 4.9$; $p = 0.016$). After conjugation with CTB, protocells proved effective to deliver YO-PRO-1 cargo into motoneuron-like NSC-34 cells, as established by the amount of intracellular YO-PRO-1 fluorescence.

3.5. CTB-protocells exhibit low toxicity to motoneurons

Cultured motoneurons were incubated with different concentrations of CTB-protocells for different times (up to 24 h). Dead cells were identified by dead-cell protease activity using a luminogenic peptide substrate, and the total number of cells was determined following addition of a lysis reagent. There was no difference across treatment groups in the percent of dead cells ($F_{5,42} = 2.2$; $p = 0.077$); however, there was a difference in luminescence following cell lysis ($F_{5,42} = 12.3$; $p < 0.001$). Incubation with 25 μg/ml of CTB-protocells for 3 h decreased total cell luminescence while incubation with 50 μg/ml of CTB-protocells for 24 h increased total cell luminescence (Fig. 8A). Since the number of total cells is dependent on the toxicity of the protocell and degree of impairment in proliferation, we evaluated a greater protocell concentration (50 μg/ml) for the same incubation time (3 h) to see if the decrease observed at 3 h was caused by protocell toxicity. There was no difference in total number of cells compared to control. We also looked at cell proliferation impairments at 24 h using a cell proliferation assay. Cell number determined by DNA content showed no evidence of an effect on

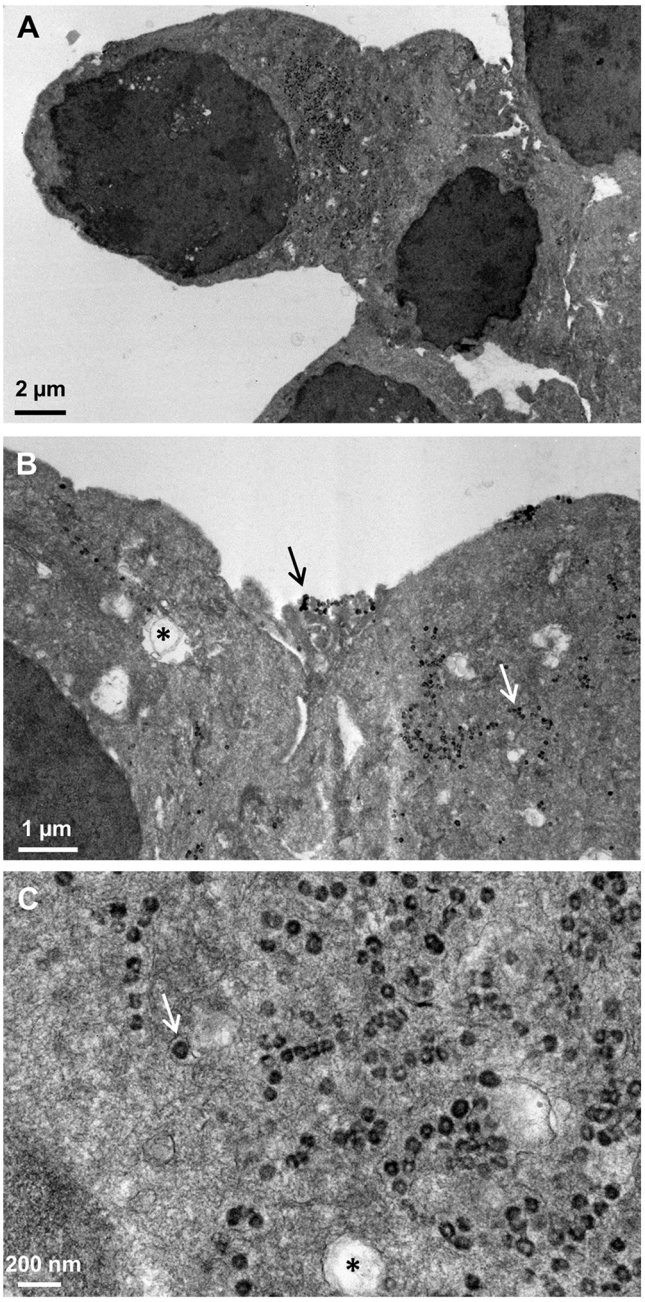

Fig. 4. TEM images of cultured NSC-34 motoneuron-like cells. (A) Internalization of CTB-protocells in NSC-34 motoneuron-like cells after 24 h incubation. (B) CTB-protocells were observed in the cell periphery as well as in the cytoplasm. Arrows highlight representative membrane-bound and internalized CTB-protocells. Asterisk highlights an intracellular vacuole (note presence of membrane). (C) Higher magnification image showing internalized particles (arrow) outside vacuoles compartments (asterisk).

cell proliferation or viability after 24 h of treatment with 50 µg/ml of CTB-protocells, compared to untreated cells (Fig. 8B).

3.6. CTB-protocell mediated uptake at motoneuron axon terminals

To evaluate the specificity of CTB-protocells targeting of motoneurons, the uptake at the NMJ was assessed. Hemi-diaphragm preparations were treated acutely with either CTB modified or unmodified protocells. Using confocal imaging, we measured changes in protocell fluorescence at the NMJ. After 24 h incubation with CTB-protocells we observed a substantial protocell fluorescent intensity increase in each NMJ compared to unmodified protocells and no treatment (Fig. 9C). In order to count the number of positive NMJs (NMJs with protocells), we selected a fluorescent intensity threshold based on the control fluorescence (NMJ without treatment). Based on the maximum fluorescence in the control NMJs, 40% of the total NMJs treated with CTB-protocells were positive (protocell fluorescence was greater than the threshold) (n = 3 diaphragms per group and ~40 NMJs per diaphragm) and 6% of the NMJs treated with unmodified protocells were positive (137 NMJs from n = 3 different animals) (Fig. 9D). In an effort to quantitatively assess the extent of CTB-protocells in pre-synaptic structures, the relative volume of apposition was also determined. Overall, from the 40% CTB-protocell positive population of NMJs, the total pre-synaptic volume occupied by protocells was 8.5%. No internalization in surrounding muscle fibers was observed. NMJ planar area was measured in two-dimensional projections using the maximum intensity projection algorithm available in MetaMorph software.

4. Discussion

The current study presents a novel drug delivery system to specifically target motoneurons, *viz* CTB-modified mesoporous silica-supported lipid bilayer nanoparticles (protocells). CTB-protocells demonstrate primarily uptake at cultured motoneurons (compared to muscle cells), effective intracellular delivery of a small molecule cargo, as well as uptake by presynaptic axon terminals at diaphragm NMJs in tissue preparations. The availability of effective vehicles to target motoneurons fills an important medical need for the treatment of neuromuscular disorders given that current treatments are limited and hindered by bioavailability and off-target effects (Edupuganti et al., 2012a; Lee et al., 2013). For example, it is well known that neurotrophins can have neuroprotective, neurorestorative and stimulatory effects on diseased neurons (Numakawa et al., 2010; Weishaupt et al., 2012; Yoshii and Constantine-Paton, 2010), including motoneurons. Unfortunately, neurotrophins have a short *in vivo* half-life and insignificant passage across the blood brain barrier, leading to low concentrations at the desired sites of action (Ruozi et al., 2012; Zuccato and Cattaneo, 2009). In addition, neurotrophins can have undesirable, off-target effects since they contribute to the development of neuropathic pain *via* effects on dorsal horn neurons, in particular in inflammatory pain conditions (Constandil et al., 2011; Lin et al., 2011). Therefore, the development of a nanoparticle-based delivery platform that specifically target motoneurons could provide flexibility in potential treatment approaches including neurotrophin treatment.

Different targeting strategies have been developed for plasmid and drug delivery to neurons (Edupuganti et al., 2012a; Eleftheriadou et al., 2014; Lee et al., 2013; Rogers et al., 2014; Townsend et al., 2007). Motoneuron targeting strategies involve surface incorporation of ligands (*e.g.*, antibodies against p75NTR) or atoxic subunits (*e.g.*, atoxic subunits of botulinum neurotoxin or tetanus toxin) that bind specifically to motoneurons at the NMJ, exploiting retrograde motoneuron transport. Although these drug delivery systems are promising, the functionality of the vehicles to load and deliver cargo in motoneurons remains to be addressed. CTB was chosen as the targeting approach since it has been used extensively as a neuronal tracer because of preferential uptake by neurons (Alisky et al., 2002) and efficient retrograde transport in many species (Lencer et al., 1999).

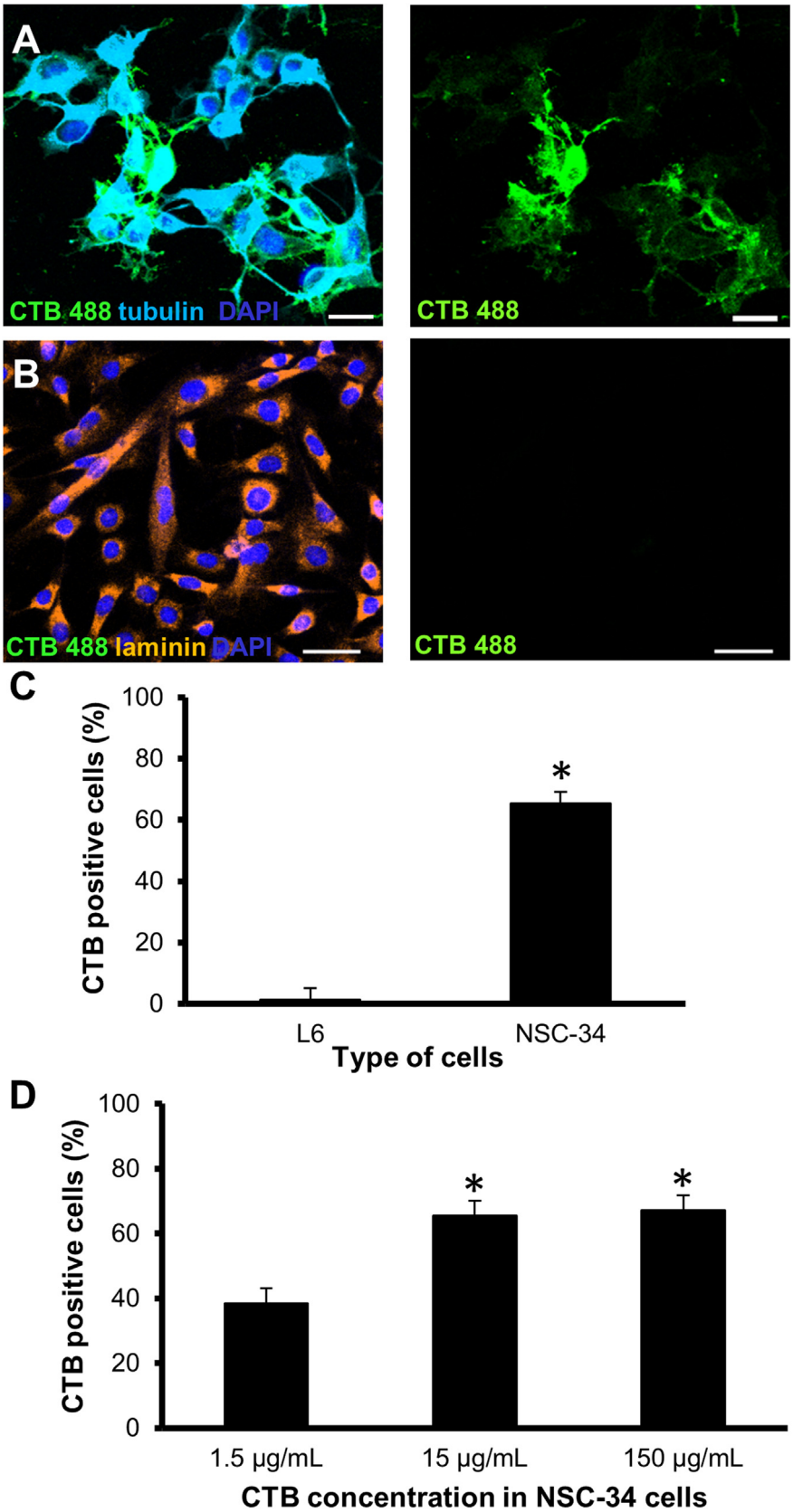

Fig. 5. Selective uptake of CTB in NSC-34 motoneuron-like cells and L6 muscle cells. Single plane confocal images of (A) NSC-34 motoneuron-like cells and (B) L6 muscle cells treated with 15 μg/ml of Alexa 488 cholera toxin subunit B (CTB) show co-localization of CTB (green) to tubulin-labeled (cyan) NSC-34 cells but not in laminin-labeled (orange) L6 cells; bar 20 μm. (C) The percentage of cells displaying CTB uptake was significantly higher in NSC-34 motoneuron-like cells compared to L6 muscle cells (*, $p < 0.001$). (D) Increasing CTB concentration in NSC-34 motoneuron-like cells did not increase uptake further. Mean ± SE values were obtained from 2 different experiments, ~600 NSC-34 cells and ~1000 L6 cells counted per group. (For interpretation of the references to colour in this figure legend, the reader is referred to the web version of this article.)

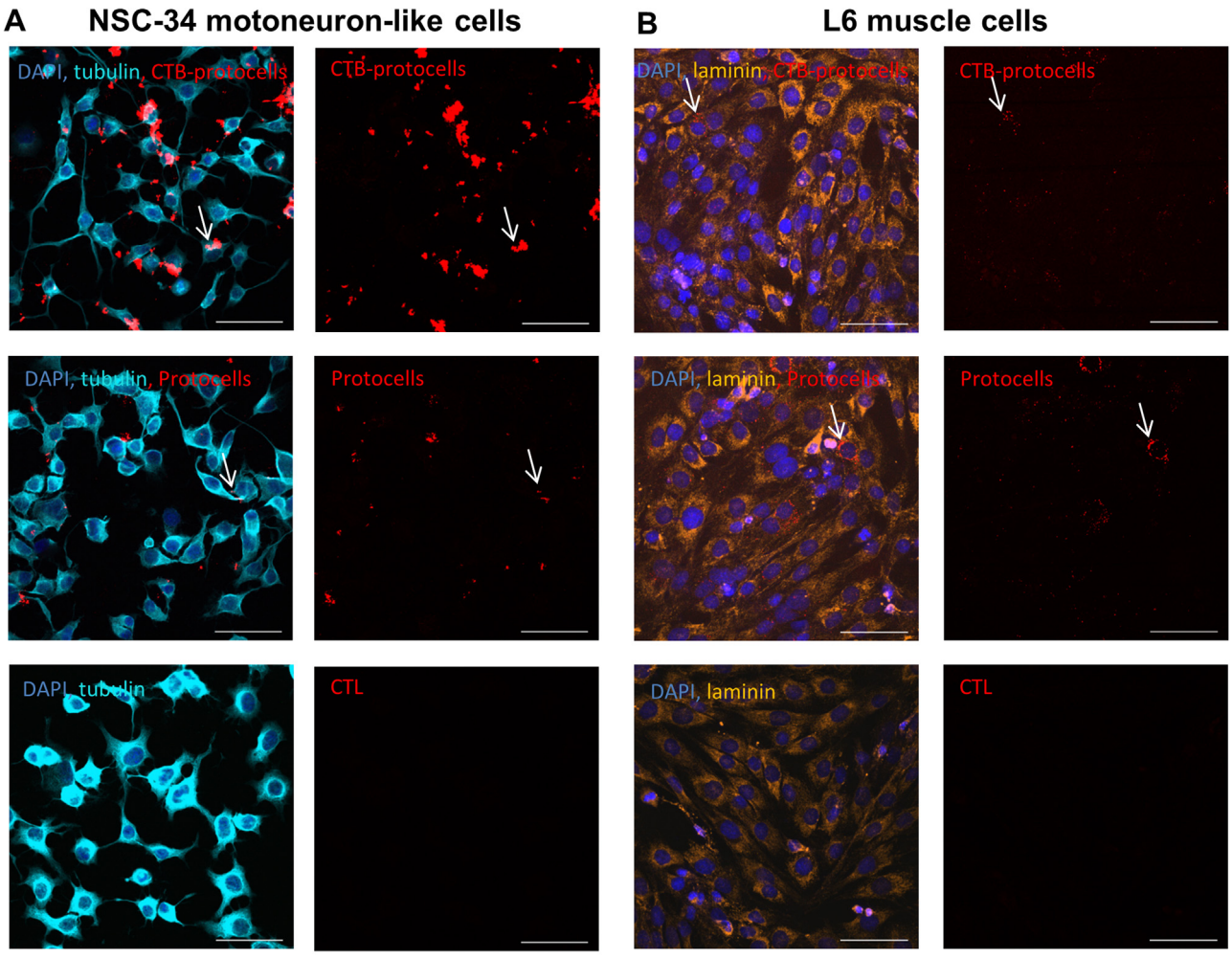

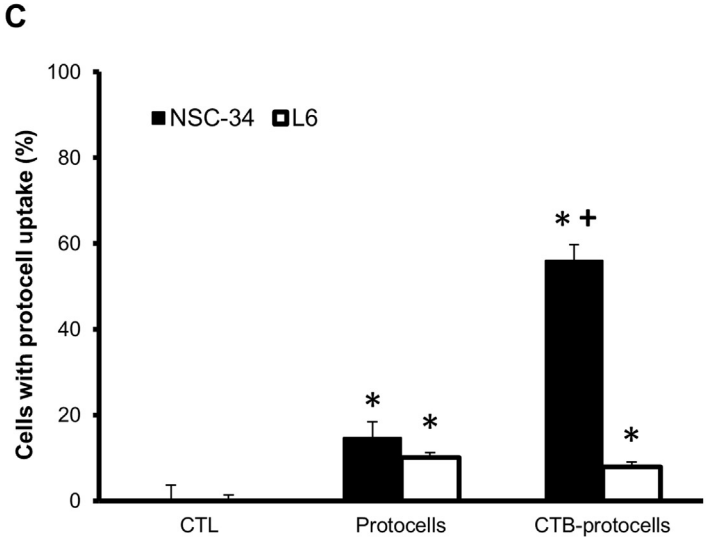

Fig. 6. Selective uptake of CTB-protocells in NSC-34 motoneuron-like cells and L6 muscle cells. Single plane confocal images of (A) cultured NSC-34 cells and (B) cultured L6 muscle cells incubated with CTB modified and unmodified protocells (both rhodamine labeled); bar 50 μm. Arrows indicate intracellular uptake of CTB-protocells or protocells. Staining of beta III tubulin identifies differentiated motoneurons while laminin staining identifies muscle cells. (C) After 24 h of incubation with protocells, the percentage of NSC-34 cells displaying protocell uptake increased for CTB-protocells compared to unmodified protocells. L6 muscle cells displayed low levels of protocell uptake, and there was no difference with CTB coating (*, $p < 0.001$ compared to untreated control (CTL) in the same cell type; $^{+}$, $p < 0.001$ compared to protocells in NSC-34 cells). Mean ± SE values were obtained from three separate experiments carried out in duplicate.

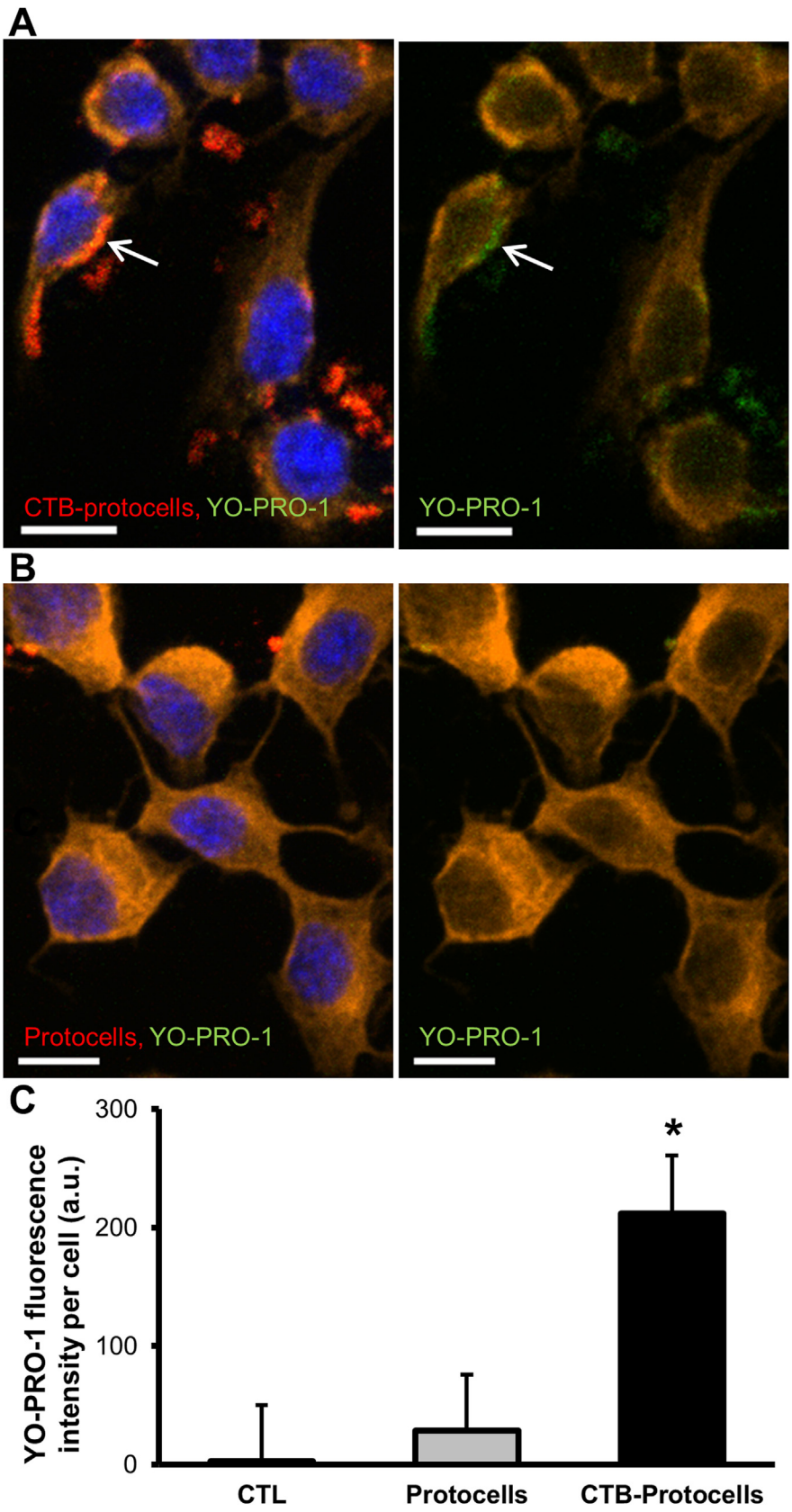

Fig. 7. YO-PRO-1 cargo release in NSC-34 motoneuron-like cells. Single plane confocal images of cultured NSC-34 cells treated for 24 h with (A) 50 μg/ml of YO-PRO-1 loaded CTB-protocells and (B) 50 μg/ml of YO-PRO-1 loaded unmodified protocells; bar 10 μm. Note presence of CTB-protocells (red) and YO-PRO-1 (green) in cultured NSC-34 cells (arrow), which are co-stained with DAPI to show nuclei. (C) Intracellular YO-PRO-1 was quantified by the amount of intracellular YO-PRO-1 fluorescence. Mean ± SE values were obtained from three separate experiments (*, $p = 0.034$ compared to CTL and protocells). (For interpretation of the references to colour in this figure legend, the reader is referred to the web version of this article.)

4.1. Protocell synthesis

Targeted nanoparticle-based drug delivery systems hold the promise of precise administration of therapeutic cargos to specific cells or tissues, sparing collateral damage to non-targeted cells/tissues and potentially overcoming multiple drug resistance mechanisms (Bertrand et al., 2014; Sun et al., 2014; Tarn et al., 2013). The modular design of the protocell platform offers the unique ability to modify independent features for specific applications. In the present study, protocells were assembled by encapsulating hexagonal prismatic MSNP cores, loaded with YO-PRO-1, within a zwitterionic lipid bilayer. YO-PRO-1, was chosen as a surrogate drug to load the MSNPs since it is a small, membrane impermeable fluorescent molecule. It is important to note that the lipid bilayer composition modifies cargo loading characteristics of MSNPs. For instance, a zwitterionic liposomal formulation (*e.g.*, DSPC) will likely be more useful in loading and sealing positively charged cargos, as we demonstrated with YO-PRO-1 cargo. Positive lipid bilayers (*e.g.*, DOTAP) can increase plasmid cargo loading (due to electrostatic interactions with negatively-charged DNA). Future studies could exploit these characteristics to deliver plasmids to motoneurons. The supported lipid bilayer composition plays a critical role in the introduction of ligands to target specific receptors in a cell. We modified a technique previously described by Durfee et.al, using amine terminated DSPE-PEG_{2000} lipids conjugated with NeutrAvidin, followed by biotin-modified CTB binding (Gonzalez Porras et al., 2016). Biotin binding proteins have previously been used to conjugate proteins to the surface of microparticles and nanoparticles (Nobs et al., 2006, 2004b; Townsend et al., 2007). Non-covalent interactions between biotin and NeutrAvidin are highly specific and do not involve unstable intermediates (Townsend et al., 2007). The supported lipid bilayer stabilizes the MSNP cores in high ionic strength physiological buffer conditions, and also acts as a barrier to seal membrane impermeable YO-PRO-1 cargo within the protocell construct.

4.2. In vitro *CTB-protocell motoneuron uptake and targeting specificity*

Incubating cultured motoneuron-like NSC-34 cells with CTB-protocells resulted in rapid intracellular uptake. Importantly, differentiated motoneurons in culture also showed a great extent of uptake, which was validated with both confocal and TEM images (Figs. 3 and 4, respectively), suggesting that uptake by mature, non-proliferative neurons will occur *in vivo*. Indeed, neurons are known to display active endocytic pathways important for synaptic vesicle retrieval (Saheki and De Camilli, 2012; von Zastrow and Williams, 2012). CTB binds to the epithelial cell apical membrane using its lectin-like activity (Lencer, 2004). Binding GM1 tethers the cholera toxin (CT) to the membrane and results in the association of CT with lipid rafts. The toxin exploits retrograde transport within specific cells and can be found in early and recycling endosomes, the Golgi apparatus, and the ER (Lencer and Tsai, 2003). CTB is internalized *via* a process defined as raft-dependent endocytosis, where the lipid rafts (plasma membrane microdomains enriched in cholesterol and sphingolipids) are involved in the lateral compartmentalization of molecules at the cell surface (Lajoie et al., 2009). It is possible that CTB-protocells use this internalization mechanism since the size of raft domains is highly variable and lipid rafts include larger transient confinement domains of hundreds of microns (Dietrich et al., 2002). Also, CTB-protocells could exploit the retrograde transport seen with CTB, instead of entering the *endo*-lysosomal degradation pathway as it was suggested by the lack of presence of CTB-protocells in lysosomes after 24 h of incubation (Fig. 4). These results are consistent with a recent study using MSNPs functionalized with CTB through a polyethylene glycol polymer linker that assessed intracellular trafficking in Hela cells (Walker et al., 2016). Uptake of CTB-functionalized MSNPs followed the retrograde transport pathway to the endoplasmic reticulum and Golgi apparatus, with reduced co-localization to *endo*-lysosomes. Based on this study, CTB-protocells appear to follow similar intracellular pathways avoiding lysosomal degradation and permitting cargo release.

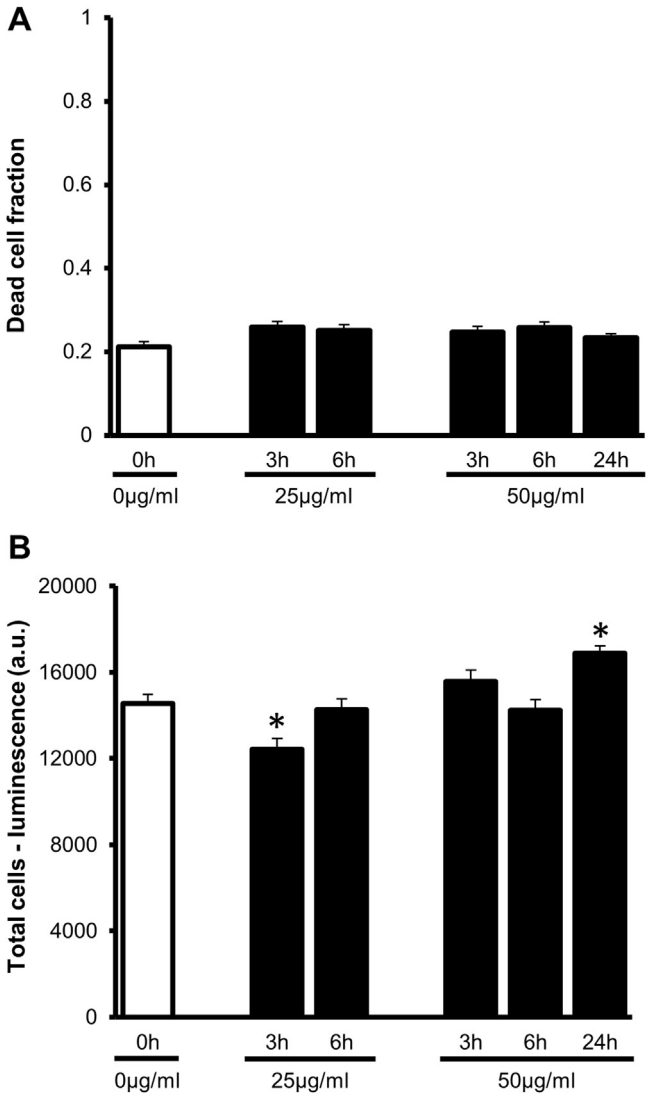

Fig. 8. Lack of CTB-protocell induced toxicity in NSC-34 motoneuron-like cells. (A) Fraction of dead cells at different CTB-protocell concentrations and incubation times. Dead cells were identified by dead-cell protease activity using a luminogenic peptide substrate. (B) Total cell luminescence determined using dead cell protease activity luminescence after addition of a lysis reagent (*, $p < 0.001$ compared to control cells). Note the lack of differences in dead cell fraction with CTB-protocell treatment and unimpaired cell proliferation evidenced by the similar or greater number of total cells following CTB-protocell treatment. Mean values ± SE were obtained from two separate experiments carried out in triplicate.

Although *in vitro* models have limitations, the NSC-34 cell line was used as a motoneuron model since these cells express many of the morphological and physiological properties of differentiated motoneurons without addition of inducing agents to the culture medium. Motoneuron-like properties include extension of neurites, formation of contacts with cultured myotubes, generation of action potentials, synthesis and storage of acetylcholine (Cashman et al., 1992) and expression of functional glutamate receptors (Eggett et al., 2000). These characteristics have permitted their use in modeling early neuromuscular synapse formation (Martinou

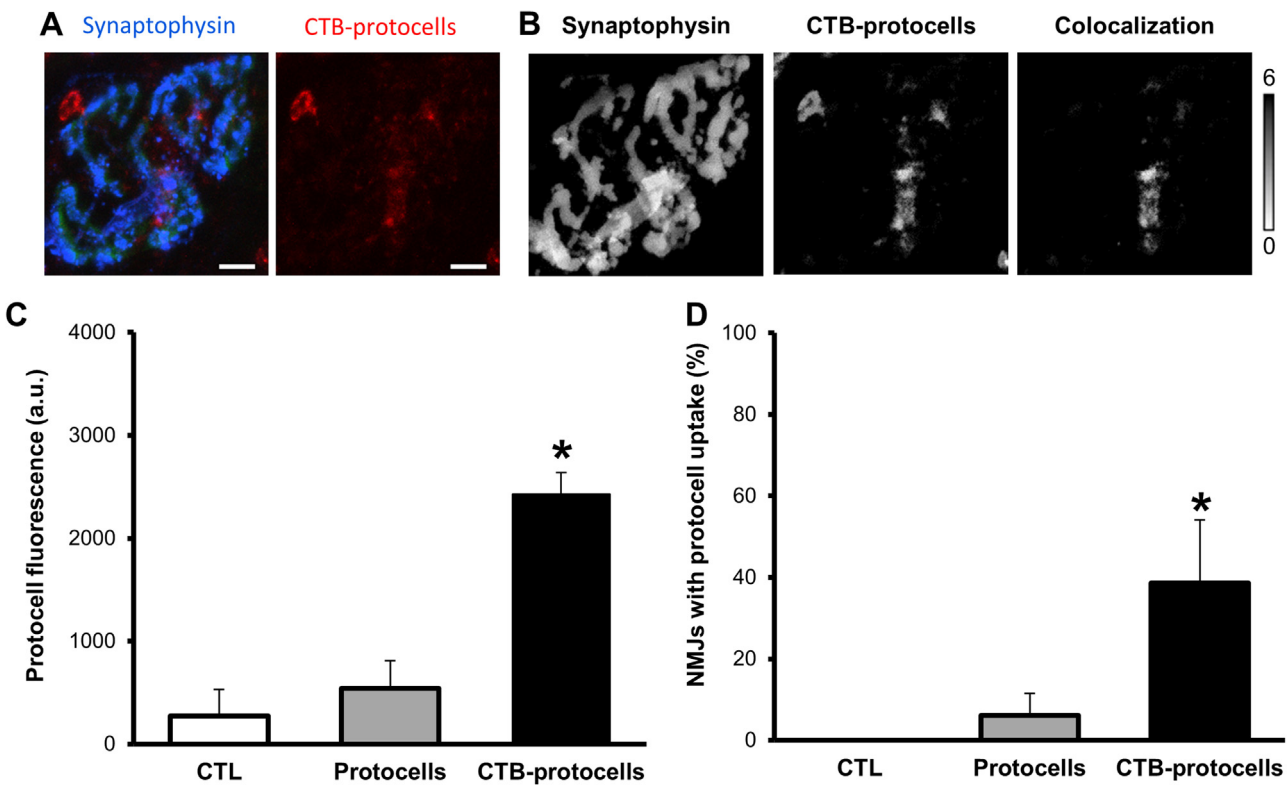

Fig. 9. CTB-protocell uptake by axon terminals at diaphragm neuromuscular junctions (NMJs). Representative (A) maximum intensity projection confocal micrographs of diaphragm muscle-phrenic nerve preparations treated with CTB-protocells, labeled with synaptophysin (axon terminal). (B) 3D reconstruction showing varying depth (grayscale, in μm) of pre-synaptic structures, CTB-protocells and presynaptic colocalization. (C) Protocell fluorescence intensity at axon terminals after 24 h incubation with CTB-protocells, unmodified protocells and no treatment (CTL). CTB-protocells had significantly greater uptake at the axon terminals compared to modified protocells (*, $p < 0.001$ compared to protocells and CTL). (D) Proportion of axon terminals displaying protocell uptake at diaphragm muscle-phrenic nerve preparations ($n = 3$ per group; ~40 NMJs per preparation). CTB-protocell uptake was determined as present at an NMJ after thresholding based on the maximum fluorescence in untreated CTL preparations.

et al., 1991; Martinou and Merlie, 1991), studying the motoneuron response to multiple growth factors (including neurotrophins) (Oppenheim, 1996; Sendtner et al., 2000; Thoenen, 1993), understanding receptor trafficking within motoneurons (Matusica et al., 2008) and investigating molecular events linked to neurodegeneration of differentiated motoneurons (Maier et al., 2013a). CTB binds to GM1 gangliosides on neuronal cell surfaces; here we confirmed GM1 presence in these cells by incubating them with Alexa 488 CTB and observing cell fluorescent labeling (Fig. 5A). In the same way we assessed CTB labeling of motoneurons compared to L6 muscle cells to establish the potential binding specificity of CTB-protocells (Fig. 5B). We confirmed the lack of CTB fluorescence in muscle cells, and thus targeting specificity (Fig. 6). The lack of CTB-protocell uptake by muscle cells supports the requirement for GM1 for both CTB and CTB-protocell uptake and the use of this toxin as a motoneuron targeting strategy (Alisky et al., 2002). The percentage of cells that had CTB-protocells uptake (~60%) was similar to the percentage of cells that were CTB labeled (~65%) suggesting that CTB-protocells are likely entering all cells with GM1 expression.

4.3. Lack of cytotoxicity by protocells

In this study, we observed that CTB-modified zwitterionic protocells showed negligible toxicity to motoneurons compared to the untreated control group where, the ~20% of dead cells was likely related to serum deprivation. Nanoparticle cytotoxicity depends on particle characteristics such as size, composition, and surface chemical effects like charge hydrophobicity and potential to generate radicals (Frohlich, 2012; Zhang et al., 2012). In addition, biological conditions including cell type, cell density, particle concentration and time of incubation play an important role in cytotoxicity. In the present study, the lack of cytotoxicity is largely a result of the conformal zwitterionic lipid bilayer that shields the underlying surface silanol (Si—OH) and ionic deprotonated silanols ($Si—O^-$) from interacting with cellular membranes. Here it should be noted that "bare" mesoporous colloidal silica has an overall low toxicity (He et al., 2011, 2009; Meng et al., 2011; Phillips et al., 2014) but does exhibit dose dependent hemolysis of RBCs that is virtually abolished by protocells (Ashley et al., 2012, 2011; Lin and Haynes, 2010). The low toxicity might also reflect the specific cell type used (motoneurons) that can survive under extreme conditions (*e.g.* neurodegenerative conditions) due to their neuroprotective mechanisms (Maier et al., 2013b; Valbuena et al., 2016).

4.4. CTB-protocells as a motoneuron cargo delivery system

Our results demonstrate that YO-PRO-1 loaded protocells were internalized by NSC-34 cells and the cargo was released intracellularly meaning that it escaped the protocell and endosomal compartment. Based on the uptake and trafficking of CTB-functionalized MSNPs to the endoplasmic reticulum and Golgi apparatus (Walker et al., 2016), CTB-protocells can be expected to avoid lysosomal degradation and thus permit release of the encapsulated cargo. However, even with *endo*-lysosomal uptake, it is likely that the acidic conditions of endosomes and lysosomes can destabilize the supported lipid bilayer of protocells (presumably due to reduced adhesion energy) allowing encapsulated cargo to diffuse out of the nanoporous core. In future applications, if there is further need to enhance endosomal escape, modifying the lipid bilayer of the protocells with a fusogenic lipid such as dioleoylphos-

phatidyl ethanolamine (DOPE) or fusogenic peptide could be used to promote endosomal escape of internalized protocells avoiding lysosomal degradation of sensitive cargos and enabling cytosolic distribution of protocell-encapsulated cargos (Ashley et al., 2012, 2011). The favorable delivery and toxicity profile renders protocells a good approach to target and deliver molecules to motoneurons *in vivo*.

4.5. CTB-protocell uptake at NMJs

By coating protocells with CTB, we developed a novel formulation that is preferentially taken up by axonal terminals at the NMJ in diaphragm tissues, as compared to surrounding muscle. The lack of skeletal muscle uptake of CTB-protocells supports that these particles might be suitable drug delivery vehicles for motoneurons. Previous studies with motoneuron targeting systems are limited to liposomal formulations (Edupuganti et al., 2012a; Lee et al., 2013). Our vehicle combines the advantages of liposomes and mesoporous silica nanoparticles and exploits a novel targeting strategy that permits large loading capacity and greater cargo release.

Our results demonstrated CTB-protocell uptake by at least 40% of the diaphragm NMJs. This level of uptake was achieved despite the lack of synaptic vesicle release and recycling associated with expected activity levels *in vivo*. Although spontaneous synaptic vesicle events associated with miniature end-plate potentials are present in the ex vivo diaphragm muscle-phrenic preparations, synaptic vesicle release and recycling is greatly enhanced by electrical stimulation (Mantilla et al., 2004; Rowley et al., 2007) It is possible that electrical stimulation of the phrenic nerve will enhance CTB-protocell uptake as membrane recycling occurs, although it is not clear whether lipid raft endocytosis is specifically enhanced at synapses as a result of synaptic activity and activity-dependent bulk endocytosis (Soykan et al., 2016). Future studies should investigate the role of the activity in the internalization of CTB-protocells at the presynaptic axon terminal.

Having a complete targeting strategy involves not only the vehicle but also the delivery method. Systemic injection of CTB has been demonstrated to label motor neurons throughout the entire rostrocaudal extent of the brain and spinal cord in a concentration dependent manner (Alisky et al., 2002). Our group has shown that intrapleural injection of CTB labels all phrenic motoneurons (Mantilla et al., 2009). Moreover, CTB can be taken up by neurons not only at terminals and dendrites, but also by axons of passage (Chen and Astonjones, 1995; Lencer, 2004), which will open the possibility to deliver cargo not only at the NMJ, but also to the axons and cell soma in the spinal cord. The specificity of CTB-protocell uptake by motoneurons suggest that with intramuscular or intrapleural delivery, targeting of muscle cells would be unlikely to occur. Next steps will look into different mechanisms of delivery *in vivo*.

5. Conclusions

In summary, CTB-protocells provide a promising delivery vehicle for therapy in motoneuron diseases and neuromuscular disorders. The ability of CTB-protocells to enter motoneurons at the NMJ confers a great advantage over existing formulations. The demonstrated biocompatibility of CTB-protocells with motoneurons suggests that CTB-protocells constitute a viable targeted cell delivery system suitable for drugs and genes. Protocell based delivery systems permit interventions, *e.g.*, in the treatment of motoneuron diseases, that can be personalized depending on disease stage and other patient and condition specific considerations. Finally, customizable nanoparticle-based drug delivery platforms can facilitate studies examining the mechanisms of motoneuron disease, muscle denervation, and neuromuscular plasticity, thus offering both promising therapeutic and diagnostic potential.

Acknowledgments

This project was supported by internal funding from the Mayo Foundation. C.J.B. acknowledges the U.S. Department of Energy (DOE), Office of Basic Energy Sciences (BES), and the Division of Materials Sciences and Engineering for support of fundamental structure-property relationship studies. C.J.B also acknowledges the Air Force Office of Scientific Research grant FA 9550-1-14-066, the National Science Foundation Grant#1344298, and the University of California's Center for Environmental Implications of Nanotechnology (CEIN) Grant # DBI-1266377.

References

Alisky, J.M., van de Wetering, C.I., Davidson, B.L., 2002. Widespread dispersal of cholera toxin subunit b to brain and spinal cord neurons following systemic delivery. Exp. Neurol. 178, 139–146.

Alvarez-Argote, S., Gransee, H.M., Mora, J.C., Stowe, J.M., Jorgenson, A.J., Sieck, G.C., Mantilla, C.B., 2016. The impact of midcervical contusion injury on diaphragm muscle function. J. Neurotrauma 33, 500–509.

Ashley, C.E., Carnes, E.C., Phillips, G.K., Padilla, D., Durfee, P.N., Brown, P.A., Hanna, T.N., Liu, J., Phillips, B., Carter, M.B., Carroll, N.J., Jiang, X., Dunphy, D.R., Willman, C.L., Petsev, D.N., Evans, D.G., Parikh, A.N., Chackerian, B., Wharton, W., Peabody, D.S., Brinker, C.J., 2011. The targeted delivery of multicomponent cargos to cancer cells by nanoporous particle-supported lipid bilayers. Nat. Mater. 10, 389–397.

Ashley, C.E., Carnes, E.C., Epler, K.E., Padilla, D.P., Phillips, G.K., Castillo, R.E., Wilkinson, D.C., Wilkinson, B.S., Burgard, C.A., Kalinich, R.M., Townson, J.L., Chackerian, B., Willman, C.L., Peabody, D.S., Wharton, W., Brinker, C.J., 2012. Delivery of small interfering RNA by peptide-targeted mesoporous silica nanoparticle-supported lipid bilayers. ACS Nano 6, 2174–2188.

Bertrand, N., Wu, J., Xu, X., Kamaly, N., Farokhzad, O.C., 2014. Cancer nanotechnology: the impact of passive and active targeting in the era of modern cancer biology. Adv. Drug Deliv. Rev. 66, 2–25.

Boido, M., Vercelli, A., 2016. Neuromuscular junctions as key contributors and therapeutic targets in spinal muscular atrophy. Front. Neuroanat., 10.

Butler, K.S., Durfee, P.N., Theron, C., Ashley, C.E., Carnes, E.C., Brinker, C.J., 2016. Protocells modular mesoporous silica nanoparticle-supported lipid bilayers for drug delivery. Small 12 (16), 2173–2185.

Cashman, N.R., Durham, H.D., Blusztajn, J.K., Oda, K., Tabira, T., Shaw, I.T., Dahrouge, S., Antel, J.P., 1992. Neuroblastoma x spinal cord (NSC) hybrid cell lines resemble developing motor neurons. Dev. Dyn. 194, 209–221.

Chen, S., Astonjones, G., 1995. Evidence that cholera-Toxin-B subunit (Ctb) can be avidly taken up and transported by fibers of passage. Brain Res. 674, 107–111.

Comley, L.H., Nijssen, J., Frost-Nylen, J., Hedlund, E., 2016. Cross-disease comparison of amyotrophic lateral sclerosis and spinal muscular atrophy reveals conservation of selective vulnerability but differential neuromuscular junction pathology. J. Comp. Neurol. 524, 1424–1442.

Constandil, L., Aguilera, R., Goich, M., Hernandez, A., Alvarez, P., Infante, C., Pelissier, T., 2011. Involvement of spinal cord BDNF in the generation and maintenance of chronic neuropathic pain in rats. Brain Res. Bull. 86, 454–459.

Dederen, P.J., Gribnau, A.A., Curfs, M.H., 1994. Retrograde neuronal tracing with cholera toxin B subunit: comparison of three different visualization methods. Histochem. J. 26, 856–862.

Dietrich, C., Yang, B., Fujiwara, T., Kusumi, A., Jacobson, K., 2002. Relationship of lipid rafts to transient confinement zones detected by single particle tracking. Biophys. J. 82, 274–284.

Dupuis, L., Loeffler, J.P., 2009. Neuromuscular junction destruction during amyotrophic lateral sclerosis: insights from transgenic models. Curr. Opin. Pharmacol. 9, 341–346.

Durfee, P.N., Lin, Y.S., Dunphy, D.R., Muniz, A.J., Butler, K.S., Humphrey, K.R., Lokke, A.J., Agola, J.O., Chou, S.S., Chen, I.M., Wharton, W., Townson, J.L., Willman, C.L., Brinker, C.J., 2016. Mesoporous silica nanoparticle-supported lipid bilayers (protocells) for active targeting and delivery to individual leukemia cells. ACS Nano.

Edupuganti, O.P., Ovsepian, S.V., Wang, J., Zurawski, T.H., Schmidt, J.J., Smith, L., Lawrence, G.W., Dolly, J.O., 2012a. Targeted delivery into motor nerve terminals of inhibitors for SNARE-cleaving proteases via liposomes coupled to an atoxic botulinum neurotoxin. FEBS J. 279, 2555–2567.

Edupuganti, O.P., Ovsepian, S.V., Wang, J.F., Zurawski, T.H., Schmidt, J.J., Smith, L., Lawrence, G.W., Dolly, J.O., 2012b. Targeted delivery into motor nerve terminals of inhibitors for SNARE-cleaving proteases via liposomes coupled to an atoxic botulinum neurotoxin. FEBS J. 279, 2555–2567.

Eggett, C.J., Crosier, S., Manning, P., Cookson, M.R., Menzies, F.M., McNeil, C.J., Shaw, P.J., 2000. Development and characterisation of a glutamate-sensitive motor neurone cell line. J. Neurochem. 74, 1895–1902.

Eleftheriadou, I., Trabalza, A., Ellison, S., Gharun, K., Mazarakis, N., 2014. Specific retrograde transduction of spinal motor neurons using lentiviral vectors

targeted to presynaptic NMJ receptors. Mol. Ther.: J. Am. Soc. Gene Ther. 22, 1285–1298.
Fanarraga, M.L., Avila, J., Zabala, J.C., 1999. Expression of unphosphorylated class III beta-tubulin isotype in neuroepithelial cells demonstrates neuroblast commitment and differentiation. Eur. J. Neurosci. 11, 517–527.
Frohlich, E., 2012. The role of surface charge in cellular uptake and cytotoxicity of medical nanoparticles. Int. J. Nanomed. 7, 5577–5591.
Gonzalez Porras, M.A., Gregory, A., Durfee, P., Brinker, C.J., Sieck, G.C., Mantilla, C.B., 2016. Cholera toxin-B coated protocells as a targeting drug delivery system to motoneurons. FASEB J., 30.
Greising, S.M., Ermilov, L.G., Sieck, G.C., Mantilla, C.B., 2015. Ageing and neurotrophic signalling effects on diaphragm neuromuscular function. J. Physiol. 593, 431–440.
He, Q., Zhang, Z., Gao, Y., Shi, J., Li, Y., 2009. Intracellular localization and cytotoxicity of spherical mesoporous silica nano- and microparticles. Small 5, 2722–2729.
He, Q., Zhang, Z., Gao, F., Li, Y., Shi, J., 2011. In vivo biodistribution and urinary excretion of mesoporous silica nanoparticles: effects of particle size and PEGylation. Small 7, 271–280.
Hepple, R.T., Rice, C.L., 2015. Innervation and neuromuscular control in ageing skeletal muscle. J. Physiol. 594 (8), 1965–1978.
Lajoie, P., Kojic, L.D., Nim, S., Li, L., Dennis, J.W., Nabi, I.R., 2009. Caveolin-1 regulation of dynamin-dependent, raft-mediated endocytosis of cholera toxin-B sub-unit occurs independently of caveolae. J. Cell. Mol. Med. 13, 3218–3225.
Lee, S., Ashizawa, A.T., Kim, K.S., Falk, D.J., Notterpek, L., 2013. Liposomes to target peripheral neurons and Schwann cells. PLoS One 8, e78724.
Lencer, W.I., Tsai, B., 2003. The intracellular voyage of cholera toxin: going retro. Trends Biochem. Sci. 28, 639–645.
Lencer, W.I., Hirst, T.R., Holmes, R.K., 1999. Membrane traffic and the cellular uptake of cholera toxin. Biochim. Biophys. Acta 1450, 177–190.
Lencer, W.I., 2004. Retrograde transport of cholera toxin into the ER of host cells. Int. J. Med. Microbiol. 293, 491–494.
Lin, Y.S., Haynes, C.L., 2010. Impacts of mesoporous silica nanoparticle size, pore ordering, and pore integrity on hemolytic activity. J. Am. Chem. Soc. 132, 4834–4842.
Lin, Y.S., Tsai, C.P., Huang, H.Y., Kuo, C.T., Hung, Y., Huang, D.M., Chen, Y.C., Mou, C.Y., 2005. Well-ordered mesoporous silica nanoparticles as cell markers. Chem. Mater. 17, 4570–4573.
Lin, Y.T., Ro, L.S., Wang, H.L., Chen, J.C., 2011. Up-regulation of dorsal root ganglia BDNF and trkB receptor in inflammatory pain: an in vivo and in vitro study. J. Neuroinflamm. 8, 126.
Liu, J., Stace-Naughton, A., Jiang, X., Brinker, C.J., 2009. Porous nanoparticle supported lipid bilayers (protocells) as delivery vehicles. J. Am. Chem. Soc. 131, 1354–1355.
Luzio, J.P., Pryor, P.R., Bright, N.A., 2007. Lysosomes: fusion and function. Nat. Rev. Mol. Cell Biol. 8, 622–632.
Maier, O., Bohm, J., Dahm, M., Bruck, S., Beyer, C., Johann, S., 2013a. Differentiated NSC-34 motoneuron-like cells as experimental model for cholinergic neurodegeneration. Neurochem. Int. 62, 1029–1038.
Maier, O., Bohm, J., Dahm, M., Bruck, S., Beyer, C., Johann, S., 2013b. Differentiated NSC-34 motoneuron-like cells as experimental model for cholinergic neurodegeneration. Neurochem. Int. 62, 1029–1038.
Mantilla, C.B., Sieck, G.C., 2009. Neuromuscular adaptations to respiratory muscle inactivity. Respir. Physiol. Neurobiol. 169, 133–140.
Mantilla, C.B., Rowley, K.L., Fahim, M.A., Zhan, W.Z., Sieck, G.C., 2004. Synaptic vesicle cycling at type-identified diaphragm neuromuscular junctions. Muscle Nerve 30, 774–783.
Mantilla, C.B., Zhan, W.Z., Sieck, G.C., 2009. Retrograde labeling of phrenic motoneurons by intrapleural injection. J. Neurosci. Methods 182, 244–249.
Mantilla, C.B., Stowe, J.M., Sieck, D.C., Ermilov, L.G., Greising, S.M., Zhang, C., Shokat, K.M., Sieck, G.C., 2014. TrkB kinase activity maintains synaptic function and structural integrity at adult neuromuscular junctions. J. Appl. Physiol. 117, 910–920.
Martinou, J.C., Merlie, J.P., 1991. Nerve-dependent modulation of acetylcholine receptor epsilon-subunit gene expression. J. Neurosci. 11, 1291–1299.
Martinou, J.C., Falls, D.L., Fischbach, G.D., Merlie, J.P., 1991. Acetylcholine receptor-inducing activity stimulates expression of the epsilon-subunit gene of the muscle acetylcholine receptor. Proc. Natl. Acad. Sci. U. S. A. 88, 7669–7673.
Matsumoto, A., Yoshino, H., Yuki, N., Hara, Y., Cashman, N.R., Handa, S., Miyatake, T., 1995. Ganglioside characterization of a cell line displaying motor neuron-like phenotype: GM2 as a possible major ganglioside in motor neurons. J. Neurol. Sci. 131, 111–118.
Matusica, D., Fenech, M.P., Rogers, M.L., Rush, R.A., 2008. Characterization and use of the NSC-34 cell line for study of neurotrophin receptor trafficking. J. Neurosci. Res. 86, 553–565.
Meng, H., Xue, M., Xia, T., Ji, Z.X., Tarn, D.Y., Zink, J.I., Nel, A.E., 2011. Use of size and a copolymer design feature to improve the biodistribution and the enhanced permeability and retention effect of doxorubicin-loaded mesoporous silica nanoparticles in a Murine Xenograft Tumor Model. ACS Nano 5, 4131–4144.
Miller, C.E., Majewski, J., Faller, R., Satija, S., Kuhl, T.L., 2004. Cholera toxin assault on lipid monolayers containing ganglioside GM1. Biophys. J. 86, 3700–3708.
Misra, A., Ganesh, S., Shahiwala, A., Shah, S.P., 2003. Drug delivery to the central nervous system: a review. J. Pharm. Pharm. Sci. 6, 252–273.
Nobs, L., Buchegger, F., Gurny, R., Allemann, E., 2004a. Current methods for attaching targeting ligands to liposomes and nanoparticles. J. Pharm. Sci. 93, 1980–1992.
Nobs, L., Buchegger, F., Gurny, R., Allemann, E., 2004b. Poly(lactic acid) nanoparticles labeled with biologically active Neutravidin (TM) for active targeting. Eur. J. Pharm. Biopharm. 58, 483–490.
Nobs, L., Buchegger, F., Gurny, R., Allemann, E., 2004c. Poly(lactic acid) nanoparticles labeled with biologically active Neutravidin for active targeting. Eur. J. Pharm. Biopharm. 58, 483–490.
Nobs, L., Buchegger, F., Gurny, R., Allemann, E., 2006. Biodegradable nanoparticles for direct or two-step tumor immunotargeting. Bioconjugate Chem. 17, 139–145.
Numakawa, T., Suzuki, S., Kumamaru, E., Adachi, N., Richards, M., Kunugi, H., 2010. BDNF function and intracellular signaling in neurons. Histol. Histopathol. 25, 237–258.
Oppenheim, R.W., 1996. Neurotrophic survival molecules for motoneurons: an embarrassment of riches. Neuron 17, 195–197.
Phillips, E., Penate-Medina, O., Zanzonico, P.B., Carvajal, R.D., Mohan, P., Ye, Y.P., Humm, J., Gonen, M., Kalaigian, H., Schoder, H., Strauss, H.W., Larson, S.M., Wiesner, U., Bradbury, M.S., 2014. Clinical translation of an ultrasmall inorganic optical-PET imaging nanoparticle probe. Sci. Transl. Med. 6.
Qiu, Y., Rojas, E., Murray, R.A., Irigoyen, J., Gregurec, D., Castro-Hartmann, P., Fledderman, J., Estrela-Lopis, I., Donath, E., Moya, S.E., 2015. Cell uptake, intracellular distribution, fate and reactive oxygen species generation of polymer brush engineered CeO2-x NPs. Nanoscale 7, 6588–6598.
Rogers, M.L., Smith, K.S., Matusica, D., Fenech, M., Hoffman, L., Rush, R.A., Voelcker, N.H., 2014. Non-viral gene therapy that targets motor neurons in vivo. Front. Mol. Neurosci. 7.
Rowley, K.L., Mantilla, C.B., Ermilov, L.G., Sieck, G.C., 2007. Synaptic vesicle distribution and release at rat diaphragm neuromuscular junctions. J. Neurophysiol. 98, 478–487.
Ruozi, B., Belletti, D., Bondioli, L., De Vita, A., Forni, F., Vandelli, M.A., Tosi, G., 2012. Neurotrophic factors and neurodegenerative diseases: a delivery issue. Int. Rev. Neurobiol. 102, 207–247.
Saheki, Y., De Camilli, P., 2012. Synaptic vesicle endocytosis. Cold Spring Harb. Perspect. Biol. 4, a005645.
Savarala, S., Ahmed, S., Ilies, M.A., Wunder, S.L., 2010. Formation and colloidal stability of DMPC supported lipid bilayers on SiO2 nanobeads. Langmuir 26, 12081–12088.
Savarala, S., Ahmed, S., Ilies, M.A., Wunder, S.L., 2011. Stabilization of soft lipid colloids: competing effects of nanoparticle decoration and supported lipid bilayer formation. ACS Nano 5, 2619–2628.
Sendtner, M., Pei, G., Beck, M., Schweizer, U., Wiese, S., 2000. Developmental motoneuron cell death and neurotrophic factors. Cell Tissue Res. 301, 71–84.
Sheikh, K.A., Deerinck, T.J., Ellisman, M.H., Griffin, J.W., 1999. The distribution of ganglioside-like moieties in peripheral nerves. Brain 122, 449–460.
Sieck, D.C., Zhan, W.Z., Fang, Y.H., Ermilov, L.G., Sieck, G.C., Mantilla, C.B., 2012. Structure-activity relationships in rodent diaphragm muscle fibers vs. neuromuscular junctions. Respir. Physiol. Neurobiol. 180, 88–96.
Silani, V., Bonifati, C., Buscaglia, M., Sampietro, A., Ghezzi, C., Scarlato, G., 1993. GangliosideGM1 expression during human spinal cord and neural crest development. Neuroreport 4, 767–770.
Simonato, M., Bennett, J., Boulis, N.M., Castro, M.G., Fink, D.J., Goins, W.F., Gray, S.J., Lowenstein, P.R., Vandenberghe, L.H., Wilson, T.J., Wolfe, J.H., Glorioso, J.C., 2013. Progress in gene therapy for neurological disorders. Nat. Rev. Neurol. 9, 277–291.
Soykan, T., Maritzen, T., Haucke, V., 2016. Modes and mechanisms of synaptic vesicle recycling. Curr. Opin. Neurobiol. 39, 17–23.
Sun, T.M., Zhang, Y.S., Pang, B., Hyun, D.C., Yang, M.X., Xia, Y.N., 2014. Engineered nanoparticles for drug delivery in cancer therapy. Angew. Chem. Int. Ed. 53, 12320–12364.
Tarn, D., Ashley, C.E., Xue, M., Carnes, E.C., Zink, J.I., Brinker, C.J., 2013. Mesoporous silica nanoparticle nanocarriers: biofunctionality and biocompatibility. Acc. Chem. Res. 46, 792–801.
Thoenen, H., 1993. Role played by neurotrophic factors in the maintenance and repair of the peripheral nervous system. Diabet. Med. 10 (Suppl. 2), 7S–9S.
Townsend, S.A., Evrony, G.D., Gu, F.X., Schulz, M.P., Brown Jr., R.H., Langer, R., 2007. Tetanus toxin C fragment-conjugated nanoparticles for targeted drug delivery to neurons. Biomaterials 28, 5176–5184.
Townson, J.L., Lin, Y.S., Agola, J.O., Carnes, E.C., Leong, H.S., Lewis, J.D., Haynes, C.L., Brinker, C.J., 2013. Re-examining the size/charge paradigm: differing in vivo characteristics of size- and charge-matched mesoporous silica nanoparticles. J. Am. Chem. Soc. 135, 16030–16033.
Valbuena, G.N., Rizzardini, M., Cimini, S., Siskos, A.P., Bendotti, C., Cantoni, L., Keun, H.C., 2016. Metabolomic analysis reveals increased aerobic glycolysis and amino acid deficit in a cellular model of amyotrophic lateral sclerosis. Mol. Neurobiol. 53, 2222–2240.
von Zastrow, M., Williams, J.T., 2012. Modulating neuromodulation by receptor membrane traffic in the endocytic pathway. Neuron 76, 22–32.
Walker, W.A., Tarannum, M., Vivero-Escoto, J.L., 2016. Cellular endocytosis and trafficking of cholera toxin B-modified mesoporous silica nanoparticles. J. Mater. Chem. B Mater. Biol. Med. 4, 1254–1262.
Wan, X.C.S., Trojanowski, J.Q., Gonatas, J.O., 1982. Cholera-toxin and wheat-germ-agglutinin conjugates as neuroanatomical probes—their uptake and clearance, transganglionic and retrograde transport and sensitivity. Brain Res. 243, 215–224.

Weishaupt, N., Blesch, A., Fouad, K., 2012. BDNF: the career of a multifaceted neurotrophin in spinal cord injury. Exp. Neurol. 238, 254–264.
Yoshii, A., Constantine-Paton, M., 2010. Postsynaptic BDNF-TrkB signaling in synapse maturation, plasticity, and disease. Dev. Neurobiol. 70, 304–322.
Zhang, R.G., Westbrook, M.L., Westbrook, E.M., Scott, D.L., Otwinowski, Z., Maulik, P.R., Reed, R.A., Shipley, G.G., 1995. The 2.4 angstrom crystal-structure of cholera-toxin-B subunit pentamer–choleragenoid. J. Mol. Biol. 251, 550–562.
Zhang, H., Dunphy, D.R., Jiang, X., Meng, H., Sun, B., Tarn, D., Xue, M., Wang, X., Lin, S., Ji, Z., Li, R., Garcia, F.L., Yang, J., Kirk, M.L., Xia, T., Zink, J.I., Nel, A., Brinker, C.J., 2012. Processing pathway dependence of amorphous silica nanoparticle toxicity: colloidal vs pyrolytic. J. Am. Chem. Soc. 134, 15790–15804.
Zuccato, C., Cattaneo, E., 2009. Brain-derived neurotrophic factor in neurodegenerative diseases. Nat. Rev. Neurol. 5, 311–322.